applied sciences

MDPI

Article

Hydrocarbon and Non-Hydrocarbon Generation Potential of Deltaic and Lagoonal Coals from Bohai Bay Basin

Jinfeng Xie, Yong Li *, Weikai Xu, Jiayao Chen and Weiqi Zhang

College of Geosciences & Surveying Engineering, China University of Mining and Technology, Beijing 100083, China; jinfeng_x@outlook.com (J.X.)
* Correspondence: liyong@cumtb.edu.cn

Abstract

Coal-derived gases are important natural gas resources, but the evolution of hydrocarbon products during coal thermal transformation remains incompletely understood. Here, two low-maturity coals from deltaic and lagoonal settings (R_o = 0.57% and 0.58%, respectively) were investigated using closed-system gold-tube pyrolysis at 300–600 °C to characterize their hydrocarbon-generation sequences, gas compositions, and carbon isotope evolution. Both coals showed a similar hydrocarbon generation sequence, comprising an oil-dominated interval at 300–350 °C, an intermediate interval characterized by light hydrocarbons and heavy hydrocarbon gases at 350–475 °C, and a methane-dominated interval above 475 °C. Maximum oil yields were 81.94 and 85.08 mg/g TOC, and maximum light hydrocarbon yields were 9.64 and 9.97 mg/g TOC for C-1 and C-2, respectively. At 600 °C, hydrocarbon gas ($C_{1–5}$) yields were 163.07 and 189.69 mL/g TOC, respectively. CO_2 was the dominant non-hydrocarbon gas, with yields of 24.93 and 32.12 mL/g TOC at 600 °C. The δ13C values of methane, ethane, and propane became lighter up to approximately 425 °C and then progressively heavier, while maintaining the normal isotope sequence of $\delta^{13}C_1 < \delta^{13}C_2 < \delta^{13}C_3$. These results delineate a common hydrocarbon generation trajectory for the two coals, with differences between the samples expressed primarily in gas generation intensity rather than in the sequence of product evolution.

Keywords: coal-derived gas; depositional environment; gold-tube pyrolysis; hydrocarbon generation potential; carbon isotope evolution; non-hydrocarbon gases

1. Introduction

Coal is important in an energy structure dominated by carbon-based fuels, natural gas and even new energy sources, and its diverse roles can be generally summarized as three-fold: (1) coal is a carbon predominantly composed deposit that is readily combustible, and it can remain a choice for power generation [1]; (2) natural gas derived from coal is widely developed in coal-bearing basins and accounts for 70% of natural gas production in China [2,3]; (3) coal gasification and liquefaction technologies are becoming increasingly mature for petroleum and natural gas supply, along with emerging underground coal gasification [4]. Due to the huge proven coal resources and requirements for lower carbon emissions, clean utilization of coal is the irreversible trend [1]. Clearly understanding the hydrocarbon generation sequences of coal is important for understanding coal transformation behaviors and further utilization.

Laboratory pyrolysis experiments are an important way to reveal hydrocarbons generated from rocks rich in organic matter. The complex macromolecular organic compounds

Academic Editor: Arcady Dyskin

Received: 21 August 2026
Revised: 18 September 2026
Accepted: 18 September 2026
Published: 20 September 2026

can be decomposed under the action of heating through branched chain cleavage, functional group loss and other physicochemical processes [5,6]. Thermal simulation experiments can be divided into closed, semi-closed (semi-open) and open systems [6]. The open system has the advantages of simple operation and high analytical efficiency. However, the influence of formation pressure and water on the samples cannot be considered [7,8]. The semi-closed system is pressurized by hydrocarbon generation; thus, it is also not conducive to fully simulating the effect of pressure [9]. The closed system can simulate conditions of high temperature and high pressure, which is more suitable for modeling actual hydrocarbon generation from organic matter [5,6,10–13]. At present, the closed systems include quartz tube thermal simulation, micro-scaled sealed vessel pyrolysis (MSSV), hydrocarbon expulsion autoclave thermal simulation and gold-tube thermal simulation closed systems [6]. The gold-tube thermal simulation experiment is one of the most widely used methods because it can simultaneously simulate the effects of temperature and pressure on the thermal evolution of organic matter [6,11,12].

Non-hydrocarbon gases are commonly found in produced natural gases and are also detected in thermal simulation experiments, although natural gases may also contain gases of inorganic origin [14]. High abundances of H_2S and CO_2 have been found in Permian and Triassic clastic carbonate reservoirs in the Western Canada Sedimentary Basin, which are likely to be the products of thermochemical sulfate reduction (TSR) [15,16]. And the gases also show carbon isotope reversal, $\delta^{13}C_1 > \delta^{13}C_2 < \delta^{13}C_3$, which are also seen in Bohai Bay Basin and Shixi gas field in the Ordos Basin [17,18]. Pyrolysis experiments can quantitatively reproduce the dynamic process of hydrocarbon generation, which is helpful for understanding carbon isotope variations in natural gases derived from coal.

In this study, gold-tube thermal simulation experiments in a closed system were conducted using two low-rank coals from Permian deltaic and lagoonal environments, in the Huanghua Depression, Bohai Bay Basin. Hydrocarbon and non-hydrocarbon gas yields and the stable carbon isotope compositions of the generated gases were analyzed over a temperature range of 300–600 °C at intervals of 25–50 °C. The results were used to characterize the hydrocarbon generation sequence, gas product evolution, and carbon isotope variations of the two coal samples under controlled pyrolysis conditions. Therefore, this study aims to compare the hydrocarbon and non-hydrocarbon generation characteristics of the deltaic and lagoonal coal samples and to clarify their hydrocarbon generation sequences, gas composition evolution and carbon isotope responses during pyrolysis.

2. Materials and Methods

2.1. Geological Setting and Sample Collection

The samples were collected from the Huanghua Depression in the Bohai Bay Basin, one of the important petroliferous basins in China [17,19,20]. The Huanghua Depression is located in the central part of the Bohai Bay Basin (Figure 1a), which is adjacent to the eastern Chengning Uplift, western Cangxian Uplift, northern Yanshan Fold Belt and southern Linqing depression [21]. Similar to the North China Craton as a whole, approximately 150 Ma of strata are missing between the Upper Ordovician and Upper Carboniferous because of the Caledonian movement [22]. The Benxi, Taiyuan, Shanxi, Shihezi, and Shiqianfeng Formations are developed in the Carboniferous–Permian succession. The Benxi and Taiyuan Formations were deposited in a marine–continental transitional environment and contain coal seams, carbonaceous mudstone, clastic rocks and carbonates. The Shanxi Formation was deposited in a deltaic environment and also contains coal seams. Then the Shihezi Formation has transformed to fluvial depositions with stable and widely distributed sandstones. The purple to red mudstones is developed in the Shiqianfeng Formation, which are the cap rocks. The petroleum systems in the Upper Paleozoic of the

Huanghua Depression are mainly sourced from the coal bearing strata and mudstone of the Taiyuan and Shanxi Formations.

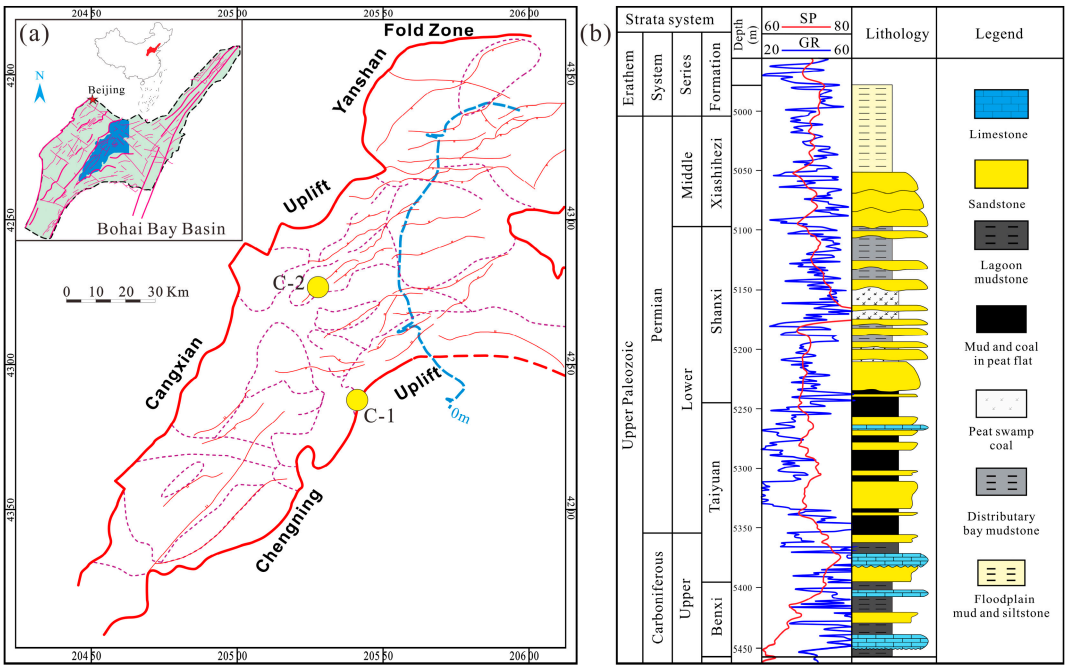

Figure 1. Geological background of the Huanghua Depression in Bohai Bay Basin. (**a**) Location of the Bohai Bay Basin and distribution of the main buried hills; (**b**) Upper Paleozoic lithology of the Huanghua Depression.

2.2. Samples

The coal samples were analyzed for TOC and routine Rock-Eval pyrolysis parameters before the gold-tube thermal simulation experiments. TOC was determined according to Chinese National Standard GB/T 19145-2022 [23], while S1, S2, S3, HI, PI and T_{max} were obtained from Rock-Eval pyrolysis analysis. The samples were collected from two coal seams in the Huanghua Depression. C-1 was a Shanxi Formation coal from the deltaic environment, and C-2 was a Taiyuan Formation coal from the lagoonal environment (Table 1). Their vitrinite reflectance (R_o) values were 0.57% and 0.58%, respectively, and their TOC contents were 78.5 wt.% and 79.5 wt.%, indicating similar initial thermal maturity and organic carbon contents. The two samples showed differences in the Rock-Eval parameters. The S2 values were 150.59 mg/g for C-1 and 201.59 mg/g for C-2, and the HI values were 191.83 and 253.57 mg/g TOC, respectively. The S1 value of C-2 was 17.83 mg/g, was substantially higher than that of C-1 (1.68 mg/g). This difference indicated that the two samples did not have identical initial hydrocarbon characteristics. Therefore, the subsequent pyrolysis results were mainly used to compare their hydrocarbon-generation processes and product changes under the same experimental conditions.

Table 1. Basic information and geochemical parameters of the coal samples used in gold-tube pyrolysis experiments.

Samples	Depth (m)	TOC (wt. %)	S_1 (mg/g)	S_2 (mg/g)	T_{max} (°C)	S_3 (mg/g)	HI (mg/g)	R_o (%)	PI
C-1	1598.57	78.5	1.68	150.59	434	4.92	191.8344	0.57	0.01
C-2	2199.52	79.5	17.83	201.59	423	5.15	253.5723	0.58	0.08

2.3. Closed-System Gold-Tube Pyrolysis

The experiments were conducted at the Key Laboratory of Petroleum Geochemistry (KLPG), PetroChina Research Institute of Petroleum Exploration and Development (RIPED), China, using a closed-system gold-tube pyrolysis apparatus. The experimental procedure followed previously reported gold-tube pyrolysis methods [6,11,14,24,25]. The samples were pulverized to 20–60 mesh, and 50 mg of each sample was encapsulated in a gold tube. The gold tubes were then loaded into the reactor and packed with metal blocks. The reactor was evacuated to minimize air contamination. The pressure was maintained at 50 MPa during the whole experimental process and was automatically controlled by a pressure pump with an uncertainty of ±0.1 MPa. The temperature uncertainty was within ±2 °C. Samples were heated at 2 °C/h to 300, 350, 375, 400, 425, 450, 475, 500, 550, and 600 °C and held at each target temperature for 12 h (Figure 2).

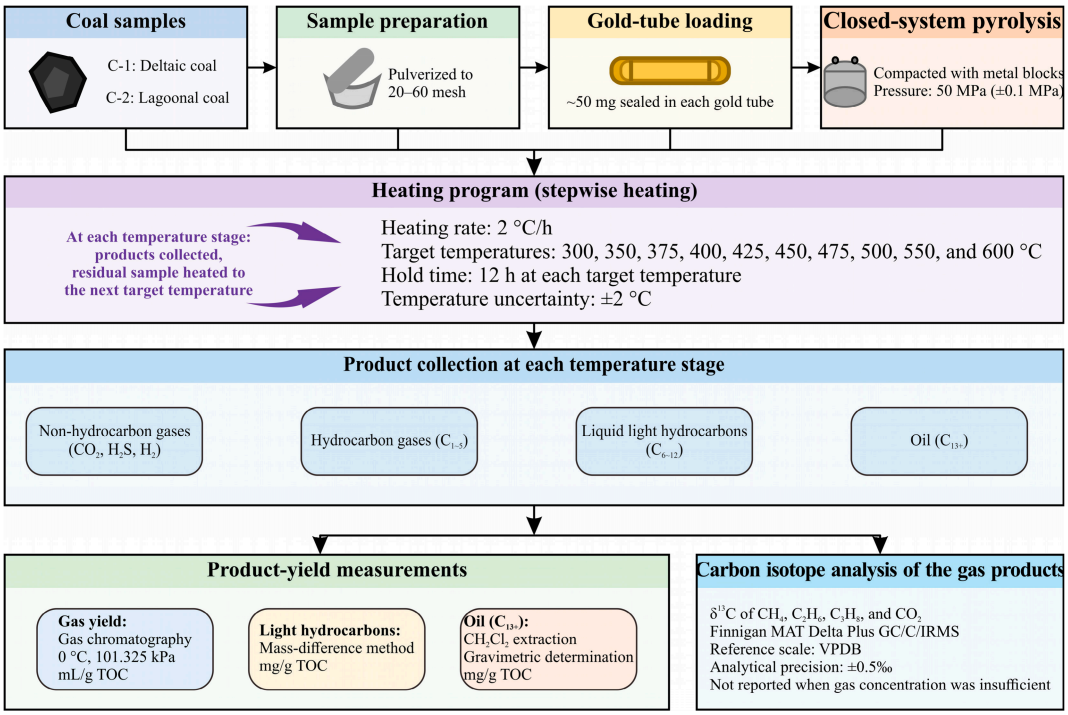

Figure 2. Experimental design of the closed-system gold-tube pyrolysis experiments.

For product yield measurements, a stepwise heating procedure was used. Products generated at each temperature stage were collected for analysis, and the residual sample was subsequently heated to the next target temperature; therefore, the reported yields represent products from each individual stage rather than cumulative products. Gas products were collected under vacuum and analyzed by gas chromatography, with volumes converted to standard conditions (0 °C and 101.325 kPa). Light hydrocarbons ($C_{6–12}$) were quantified by the mass difference method, whereas oil (C_{13+}) was recovered by CH_2Cl_2 extraction and determined gravimetrically. Liquid and gaseous yields were normalized to TOC and expressed as mg/g TOC and mL/g TOC, respectively. Following product yield measurements at each temperature stage, the corresponding gas products were further analyzed for carbon isotope compositions. The $\delta^{13}C$ values of CH_4, C_2H_6, C_3H_8, and CO_2 were measured using a Finnigan MAT Delta Plus GC/C/IRMS system. Isotope values were reported relative to VPDB with an analytical precision of ±0.5‰; values were not reported when gas concentrations were insufficient for reliable measurement. Independent replicate pyrolysis experiments and whole system mass and carbon balances were not per-

formed; therefore, the results were interpreted primarily in terms of comparative product evolution trends.

3. Results

3.1. Temperature-Dependent Evolution of Liquid Hydrocarbons

The oil fraction, defined as liquid hydrocarbons containing 13 or more carbon atoms (C_{13+}), was generated mainly at relatively low temperatures. Oil yields increased rapidly from 300 to 350 °C and reached maxima of 81.94 mg/g TOC for C-1 and 85.08 mg/g TOC for C-2, respectively, at 350 °C (Figure 3). The two samples showed similar maximum oil yields under the experimental conditions. C-2 generally showed higher oil yields at 300–375 °C, whereas C-1 was slightly higher at 400–450 °C. After 350 °C, oil yields decreased sharply and declined to low levels by 475–500 °C.

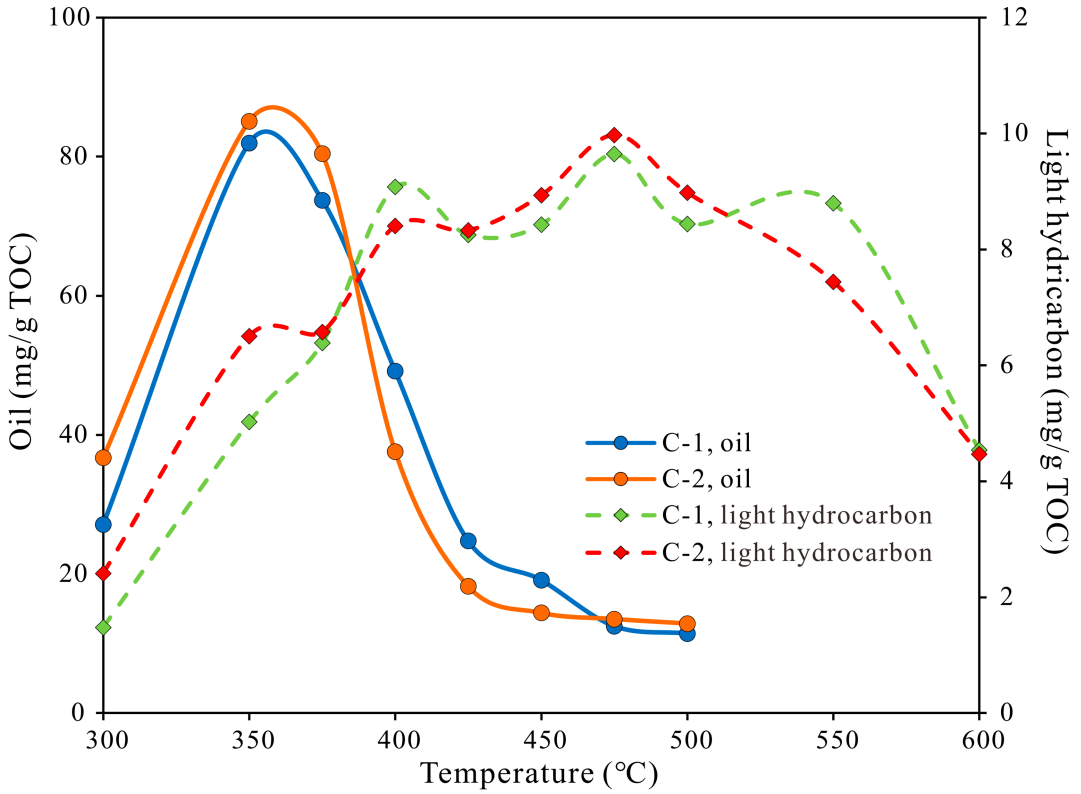

Figure 3. Yields of oil and light hydrocarbons from C-1 and C-2 at different pyrolysis temperatures.

Light hydrocarbons, defined as liquid hydrocarbons containing 6 to 12 carbon atoms ($C_{6–12}$), had much lower yields but were generated over a broader temperature range. Their maximum yields were 9.64 mg/g TOC for C-1 and 9.97 mg/g TOC for C-2, both at 475 °C. C-1 showed an early local maximum near 400 °C and a second elevated interval between 475 and 550 °C, whereas C-2 reached a pronounced maximum at 475 °C and then declined with further heating (Figure 3). Thus, the two coals had similar maximum light hydrocarbon yields but different yield patterns with temperature.

The appearance of the recovered liquid products also changed with pyrolysis temperature (Figure 4). For both samples, the oils darkened from brown to dark brown or nearly black between 300 and 350–375 °C and then became lighter and more transparent above 425 °C, consistent with decreasing oil yields. The light hydrocarbon fractions were generally lighter in color, became more evident at 350–400 °C, and gradually faded at higher temperatures. C-2 showed slightly darker light hydrocarbon products than C-1 at

350–375 °C, while the visual differences between the two samples became less distinct at higher temperatures.

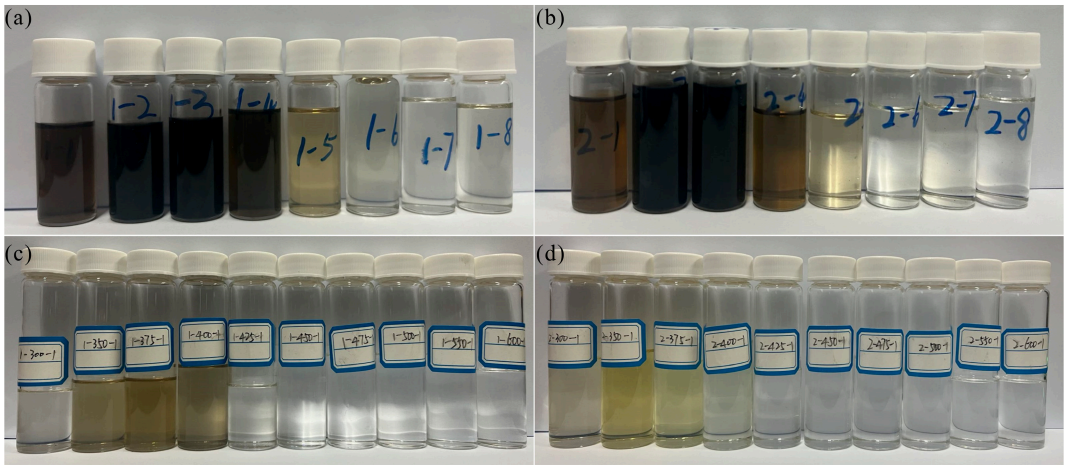

Figure 4. Photographs of the recovered oil and light hydrocarbons at different pyrolysis temperatures. (**a**) oil from C-1 (deltaic coal); (**b**) oil from C-2 (lagoonal coal); (**c**) light hydrocarbons from C-1 (deltaic coal); (**d**) light hydrocarbons from C-2 (lagoonal coal). The markers in the figure indicate various temperature points.

Although the two coals showed similar light hydrocarbon yields, the relative proportions of individual compounds varied with temperature, which may account for the differences in the color of the recovered liquid products. The distributions of selected compounds identified in the liquid $C_{6–12}$ fraction are shown in Figure 5. At 300–375 °C, C-1 contained relatively high proportions of ethylbenzene and trimethylbenzene, whereas methylcyclohexane and xylenes were more abundant in C-2. Between 425 and 500 °C, xylenes and methylbenzene showed relatively high proportions in C-1, while methylbenzene was particularly abundant in C-2 at 450–550 °C. At higher temperatures, the relative proportion of trimethylbenzene increased in C-1, whereas the selected compounds in C-2 generally decreased.

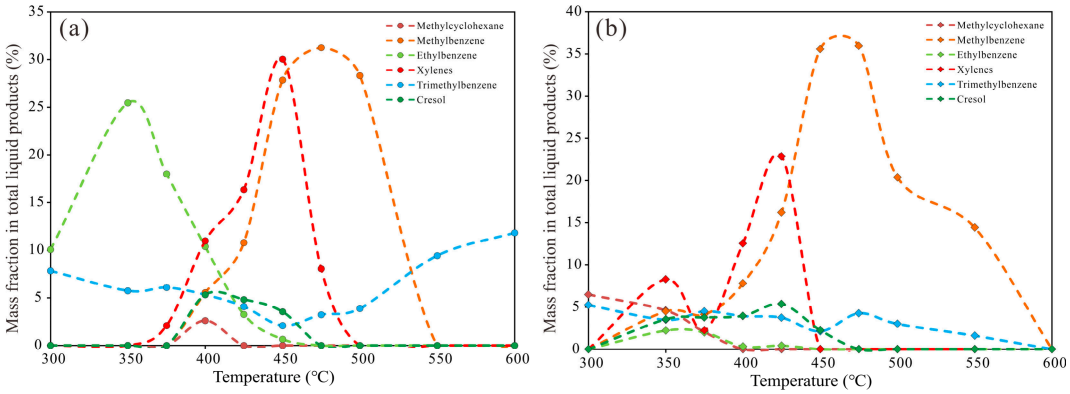

Figure 5. Relative proportions of selected compounds identified in the liquid $C_{6–12}$ fraction at different pyrolysis temperatures. (**a**) deltaic coal (C-1); (**b**) lagoonal coal (C-2). The selected compounds include methylcyclohexane, methylbenzene, ethylbenzene, xylenes, trimethylbenzene, and cresol. The relative proportion of each compound represents its mass fraction in the total light hydrocarbon ($C_{6–12}$) products.

3.2. Yields of Hydrocarbon and Non-Hydrocarbon Gases

The yields of methane (CH_4), ethane (C_2H_6), propane (C_3H_8), butane (i- + n-C_4), pentane (i- + n-C_5), and non-hydrocarbon gases (H_2, CO_2, and H_2S) produced by the

two samples are shown in Table 2 and Figure 6. The gaseous products comprise hydrocarbons ($C_{1–5}$), CO_2, H_2S and H_2. Total hydrocarbon gas is defined as $C_{1–5}$, heavy hydrocarbon gas as $C_{2–5}$, and total gas as the sum of $C_{1–5}$, H_2, CO_2, and H_2S. Total gas yields increased continuously with pyrolysis temperature in both samples, with C-2 consistently yielding more gas than C-1 (Figure 6a).

Table 2. Gas product yields from gold-tube pyrolysis experiments.

T (°C)	Product Yields	Gas Component Yield (mL/g TOC)									
		H_2	CO_2	H_2S	CH_4	C_2H_6	C_3H_8	i-C_4H_{10}	n-C_4H_{10}	i-C_5H_{12}	n-C_5H_{12}
C-1											
300	1.12		0.8946		0.1646	0.0645					
350	5.92	0.0082	3.8559		1.7414	0.2609	0.0460	0.0003	0.0030	0.0006	0.0003
375	15.58	0.0817	8.9455		5.5641	0.8946	0.0897	0.0009	0.0010	0.0008	0.0006
400	31.71	0.2712	12.3049	0.1057	15.4650	2.0623	1.2709	0.0143	0.1582	0.0385	0.0203
425	46.31	0.4883	14.2450	0.1206	24.9424	4.1638	1.9356	0.0322	0.2519	0.1005	0.0314
450	58.73	0.7286	15.0563	0.2042	35.3647	5.7945	1.3713	0.0255	0.1389	0.0482	
475	76.43	0.9795	16.4517	0.3716	52.9397	5.1664	0.4966	0.0096	0.0093	0.0011	0.0002
500	104.63	1.3121	17.3331	0.4175	81.0068	4.3831	0.1701	0.0027	0.0011	0.0002	
550	144.58	1.8451	19.1565	0.4260	122.5749	0.5653	0.0136	0.0002			
600	191.04	2.4830	24.9327	0.5477	162.7718	0.2971	0.0039				
C-2											
300	1.13		0.8643		0.2119	0.0355	0.0128	0.0006	0.0034	0.0033	0.0012
350	9.27	0.0239	6.0520	0.0120	2.3651	0.6147	0.1660	0.0019	0.0219	0.0052	0.0036
375	22.81	0.1091	11.8952	0.1260	7.2285	2.4175	0.8375	0.0096	0.1300	0.0314	0.0221
400	38.61	0.2943	14.5502	0.2809	16.4674	4.8287	1.7501	0.0200	0.3016	0.0678	0.0494
425	60.69	0.5318	17.5439	0.3516	31.8459	7.4708	2.4332	0.0283	0.3619	0.0706	0.0478
450	87.03	0.8584	20.4271	0.3584	54.1535	9.0841	1.9658	0.0222	0.1400	0.0153	0.0064
475	91.10	0.6054	19.7663	0.3568	66.1081	3.8968	0.3604	0.0040	0.0061	0.0006	0.0006
500	125.58	1.5622	22.7244	0.4154	96.5539	4.2336	0.0877	0.0007	0.0023	0.0008	0.0009
550	165.30	2.1654	24.5037	0.4169	137.9936	0.2037	0.0087	0.0002	0.0023	0.0010	0.0006
600	225.25	2.9760	32.1236	0.4647	189.5658	0.1198	0.0011				

At 600 °C, the total gas yields were 191.04 mL/g TOC for C-1 and 225.25 mL/g TOC for C-2, respectively. Hydrocarbon gases were the dominant products, with total $C_{1–5}$ yields of 163.07 mL/g TOC for C-1 and 189.69 mL/g TOC for C-2. Methane was the major hydrocarbon component and increased continuously with increasing temperature, reaching 162.77 mL/g TOC for C-1 and 189.57 mL/g TOC for C-2 at 600 °C (Figure 6a). In contrast, the yields of heavy hydrocarbon gases ($C_{2–5}$) were much lower and showed a single-peaked trend with temperature.

The total heavy hydrocarbon gas ($C_{2–5}$) yields peaked at 7.38 mL/g TOC for C-1 and 11.23 mL/g TOC for C-2 at 450 °C (Figure 6c,d). Ethane was the dominant heavy hydrocarbon gas component, with maximum yields of 5.79 mL/g TOC for C-1 and 9.08 mL/g TOC for C-2, both at 450 °C. Propane reached maximum yields at 425 °C, with values of 1.94 mL/g TOC for C-1 and 2.43 mL/g TOC for C-2. The yields of butanes and pentanes were comparatively low and decreased at higher temperatures.

Non-hydrocarbon gases were dominated by CO_2, whereas H_2 and H_2S were minor components (Figure 6b). At 600 °C, CO_2 yields were 24.93 mL/g TOC for C-1 and 32.12 mL/g TOC for C-2, which were substantially higher than the corresponding H_2 yields of 2.48 and 2.98 mL/g TOC and H_2S yields of 0.55 and 0.46 mL/g TOC, respectively. C-2 showed higher yields of hydrocarbon gases, non-hydrocarbon gases, and total gas than C-1 under the same experimental conditions (Figure 6b, Table 2).

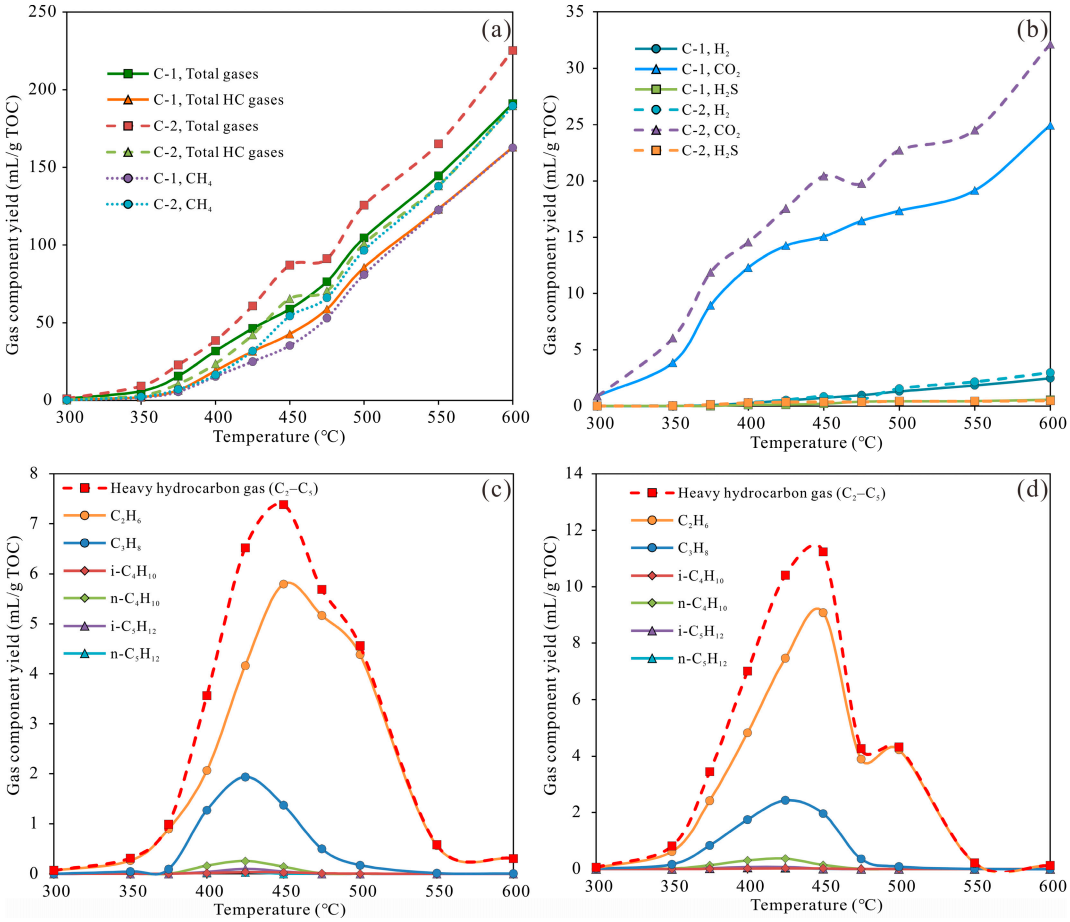

Figure 6. Characteristics of gas component yields. (**a**) Total gas and total hydrocarbon gas yields of C-1 and C-2; (**b**) non-hydrocarbon gas yields; (**c**) heavy hydrocarbon gas yield of C-1; (**d**) heavy hydrocarbon gas yield of C-2. Total gas = $C_{1–5}$ + H_2 + CO_2 + H_2S; total hydrocarbon gas = $C_{1–5}$; heavy hydrocarbon gas = $C_{2–5}$. All gas yields are expressed as mL/g TOC.

3.3. Pyrolysis Gases Generated at Different Temperatures

The relative proportions of hydrocarbon gases (CH_4, C_2H_6, C_3H_8, i-C_4H_{10}, n-C_4H_{10}, i-C_5H_{12}, n-C_5H_{12}) and non-hydrocarbon gases (H_2, CO_2 and H_2S) in the pyrolysis products at different temperatures are shown in Table 3 and Figure 7. With increasing temperature, methane became progressively dominant in the gaseous products of both samples. The relative abundance of methane increased from 14.65% at 300 °C to 85.20% at 600 °C for C-1 and from 18.71% to 84.16% for C-2. In contrast, the relative abundances of heavy hydrocarbon gases ($C_{2–5}$) were highest at intermediate temperatures and decreased markedly at higher temperatures.

The drying coefficient was defined as the ratio of methane content to the total hydrocarbon gas content, which mainly comprises methane, ethane, propane, butanes, and pentanes, and was calculated as $C_1/(C_1 + C_2 + C_3 + C_4 + C_5) \times 100\%$. It showed different trends at low to intermediate temperatures for the two samples. For C-1, the coefficient increased from 71.84% at 300 °C to 84.93% at 375 °C, then decreased to 79.29% at 425 °C. For C-2, it decreased from 78.88% at 300 °C to a minimum of 67.70% at 375 °C before increasing continuously with further heating. Above 425 °C, the drying coefficient of both samples increased rapidly and reached 99.82% for C-1 and 99.94% for C-2 at 600 °C, showing that methane became increasingly dominant in the hydrocarbon gas composition (Table 3).

Table 3. Relative abundances of gas products from the two coal samples in gold-tube pyrolysis experiments.

C-1	Main Gas Components (%)										Drying Coefficient
T (°C)	H_2	CO_2	H_2S	CH_4	C_2H_6	C_3H_8	i-C_4H_{10}	n-C_4H_{10}	i-C_5H_{12}	n-C_5H_{12}	
300	0.00	79.61	0.00	14.65	5.74	0.00	0.00	0.00	0.00	0.00	71.84
350	0.14	65.17	0.00	29.43	4.41	0.78	0.00	0.05	0.01	0.01	84.85
375	0.52	57.42	0.00	35.72	5.74	0.58	0.01	0.01	0.01	0.00	84.93
400	0.86	38.80	0.33	48.77	6.50	4.01	0.04	0.50	0.12	0.06	81.27
425	1.05	30.76	0.26	53.86	8.99	4.18	0.07	0.54	0.22	0.07	79.29
450	1.24	25.64	0.35	60.21	9.87	2.33	0.04	0.24	0.08	0.00	82.74
475	1.28	21.53	0.49	69.27	6.76	0.65	0.01	0.01	0.00	0.00	90.31
500	1.25	16.57	0.40	77.42	4.19	0.16	0.00	0.00	0.00	0.00	94.67
550	1.28	13.25	0.29	84.78	0.39	0.01	0.00	0.00	0.00	0.00	99.53
600	1.30	13.05	0.29	85.20	0.16	0.00	0.00	0.00	0.00	0.00	99.82
C-2											
300	0.00	76.29	0.00	18.71	3.14	1.13	0.05	0.30	0.29	0.10	78.88
350	0.26	65.31	0.13	25.52	6.63	1.79	0.02	0.24	0.06	0.04	74.41
375	0.48	52.16	0.55	31.69	10.60	3.67	0.04	0.57	0.14	0.10	67.70
400	0.76	37.68	0.73	42.65	12.51	4.53	0.05	0.78	0.18	0.13	70.12
425	0.88	28.91	0.58	52.48	12.31	4.01	0.05	0.60	0.12	0.08	75.36
450	0.99	23.47	0.41	62.22	10.44	2.26	0.03	0.16	0.02	0.01	82.82
475	0.66	21.70	0.39	72.56	4.28	0.40	0.00	0.01	0.00	0.00	93.93
500	1.24	18.10	0.33	76.89	3.37	0.07	0.00	0.00	0.00	0.00	95.71
550	1.31	14.82	0.25	83.48	0.12	0.01	0.00	0.00	0.00	0.00	99.84
600	1.32	14.26	0.21	84.16	0.05	0.00	0.00	0.00	0.00	0.00	99.94

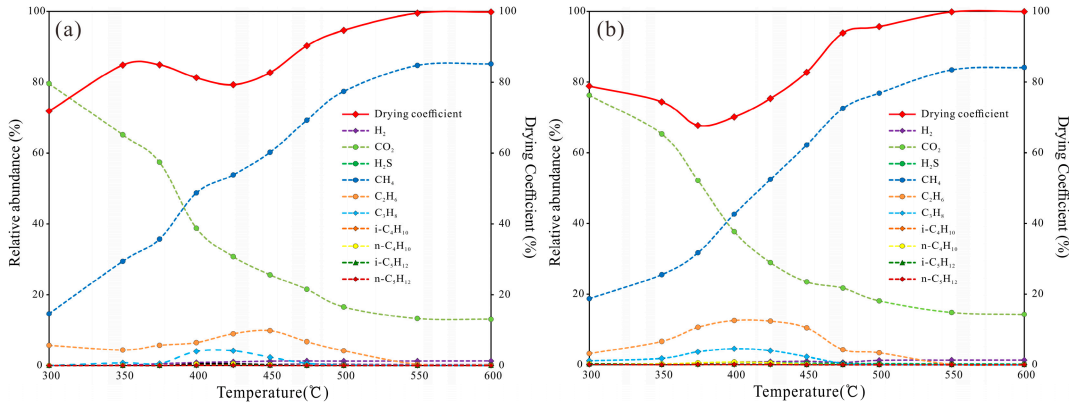

Figure 7. Relative abundances of gaseous components and the drying coefficient at different pyrolysis temperatures. (**a**) C-1; (**b**) C-2. The gaseous components include CH_4, C_2H_6, C_3H_8, i-C_4H_{10}, n-C_4H_{10}, i-C_5H_{12}, n-C_5H_{12}, H_2, CO_2 and H_2S. The drying coefficient was calculated as $C_1/(C_1 + C_2 + C_3 + C_4 + C_5) \times 100\%$.

CO_2 was the dominant non-hydrocarbon component, particularly at low temperatures. Its relative abundance decreased from 79.61% at 300 °C to 13.05% at 600 °C for C-1 and from 76.29% to 14.26% for C-2. H_2 remained a minor component but increased gradually with temperature, reaching 1.30% and 1.32% at 600 °C for C-1 and C-2, respectively. H_2S was detected at low relative abundances throughout the experiments, with relative abundances generally below 0.8%.

The differences in gas composition between the two samples were most apparent at the low- to intermediate-temperature stages. C-2 generally contained higher relative proportions of heavy hydrocarbon gases between 350 and 425 °C, whereas C-1 showed

a higher drying coefficient during most of this interval. At higher temperatures, the compositional differences between the two samples gradually diminished as methane became the dominant gaseous product.

3.4. Carbon Isotopic Compositions of Generated Gases

The carbon isotopic compositions of methane, ethane, propane, and CO_2 generated from C-1 and C-2 are summarized in Table 4 and Figure 8. At the 10 experimental temperatures, the $\delta^{13}C_1$, $\delta^{13}C_2$ and $\delta^{13}C_3$ values of both samples became progressively lighter and then heavier with increasing temperature. The $\delta^{13}C_{CO2}$ values varied within a relatively narrow range, becoming heavier at first and then slightly lighter (Table 4).

Table 4. Carbon isotope compositions of gases generated from the two coal samples during gold-tube pyrolysis experiments.

Temperature (°C)	$\delta^{13}C$ (‰, VPDB)							
	C-1				C-2			
	CO_2	CH_4	C_2H_6	C_3H_8	CO_2	CH_4	C_2H_6	C_3H_8
300	−19.86	−24.65	−23.18		−18.02	−24.34	−23.02	
350	−17.2	−26.78	−22.62	−21.25	−16.24	−26.95	−22.2	−21.35
375	−16.55	−31.65	−23.56	−22.96	−15.83	−31.45	−23.01	−22.94
400	−16.12	−35.95	−25.52	−24.25	−15.48	−35.57	−26.13	−24.75
425	−16.09	−37.65	−26.25	−24.95	−15.65	−37.95	−26.36	−25.43
450	−16.56	−31.84	−24.42	−21.27	−15.98	−32.13	−24.62	−21.85
475	−16.01	−29.59	−21.82	−19.65	−15.91	−30.56	−21.32	−19.15
500	−16.52	−28.78	−17.51		−16.33	−29.06	−15.64	
550	−16.61	−26.98	−14.21		−16.94	−25.96	−15.49	
600	−17.72	−24.62	−13.95		−17.73	−24.63	−15.46	

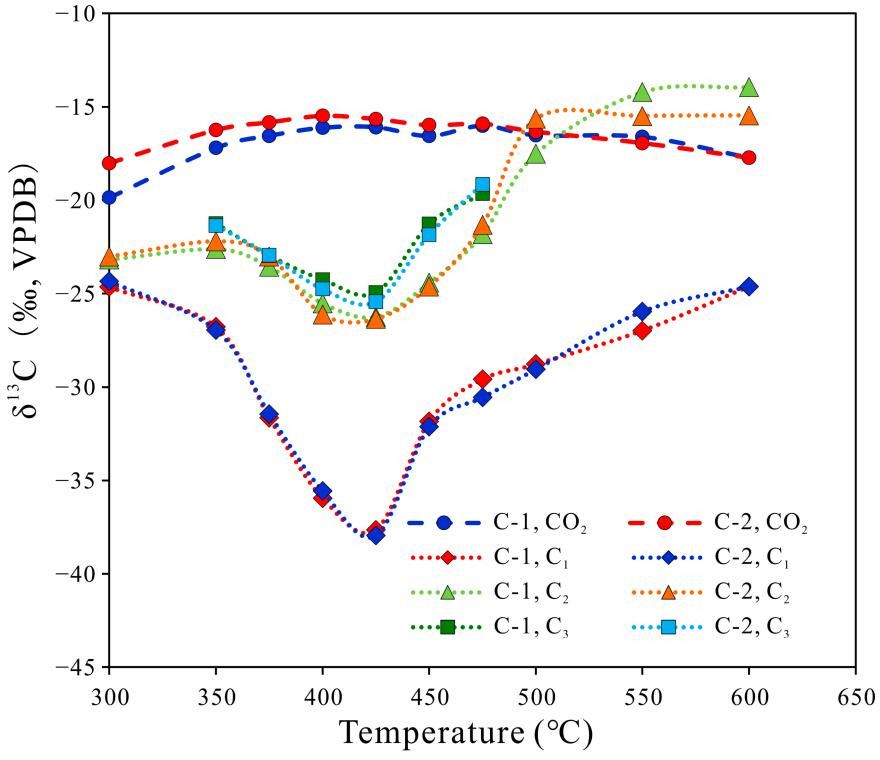

Figure 8. Carbon isotope compositions of methane, ethane, propane and CO_2 generated from the deltaic coal (C-1) and lagoonal coal (C-2) during gold-tube pyrolysis experiments.

For C-1, $\delta^{13}C_1$ ranged from −37.65‰ to −24.62‰, $\delta^{13}C_2$ ranged from −26.25‰ to −13.95‰, and $\delta^{13}C_3$ ranged from −24.95‰ to −19.65‰. For C-2, the corresponding ranges were −37.95‰ to −24.34‰, −26.36‰ to −15.46‰, and −25.43‰ to −19.15‰, respectively. The lightest carbon isotope values of methane, ethane, and propane were generally observed at 425 °C. At this temperature, $\delta^{13}C_1$ values reached −37.65‰ for C-1 and −37.95‰ for C-2, while $\delta^{13}C_2$ values reached −26.25‰ and −26.36‰, and $\delta^{13}C_3$ values reached −24.95‰ and −25.43‰, respectively. At temperatures above 425 °C, the $\delta^{13}C$ values of methane and ethane became progressively heavier in both samples. The $\delta^{13}C_1$ values reached −24.62‰ for C-1 and −24.63‰ for C-2 at 600 °C, whereas $\delta^{13}C_2$ values reached −13.95‰ and −15.46‰, respectively. The $\delta^{13}C_3$ values were only determined between 350 and 475 °C because propane concentrations at 300 °C and above 500 °C were insufficient for reliable isotope analysis.

The $\delta^{13}C_{CO2}$ values varied within relatively narrow ranges compared with those of the hydrocarbon gases. For C-1, $\delta^{13}C_{CO2}$ ranged from −19.86‰ to −16.01‰, while the corresponding range for C-2 was −18.02‰ to −15.48‰. The $\delta^{13}C_{CO2}$ values became heavier from 300 to 400 °C and then slightly lighter with further heating. Where isotope data were available for all three hydrocarbon gases, both samples maintained the normal carbon isotope sequence of $\delta^{13}C_1 < \delta^{13}C_2 < \delta^{13}C_3$.

4. Discussion

4.1. Hydrocarbon Generation Characteristics of the Two Coal Samples

The two coals showed similar maximum liquid hydrocarbon yields but different gas yields under the same experimental conditions. The maximum oil yields were 81.94 mg/g TOC for C-1 and 85.08 mg/g TOC for C-2, while the corresponding maximum light hydrocarbon yields were 9.64 mg/g TOC and 9.97 mg/g TOC, respectively. The differences in maximum liquid product yields between the two samples were relatively small. By contrast, C-2 showed higher gas yields than C-1. At 600 °C, the $C_{1–5}$ yield of C-2 was 189.69 mL/g TOC, approximately 16% higher than that of C-1 (163.07 mL/g TOC), while the total gas yields were 225.25 and 191.04 mL/g TOC, respectively, a difference of approximately 18%.

The difference between the two samples was more evident for heavy hydrocarbon gases. The maximum heavy hydrocarbon gas yield of C-2 reached 11.23 mL/g TOC at 450 °C, compared with 7.38 mL/g TOC for C-1. Ethane was the dominant heavy hydrocarbon gas component in both samples, but its maximum yield was substantially higher in C-2. The higher heavy hydrocarbon gas yields of C-2 were mainly observed at intermediate temperatures, while the liquid hydrocarbon yields of the two samples remained close.

4.2. Hydrocarbon Generation Sequences

The evolution of hydrocarbon products can be divided into three broad experimental temperature intervals according to the variations in liquid and gaseous product yields. During the 300–350 °C interval, oil was the dominant hydrocarbon product, and the oil yields of both samples reached their maximum values at 350 °C. Because C-1 and C-2 had already reached an early maturity stage before pyrolysis, the liquid products recovered at relatively low temperatures may include both thermally released retained hydrocarbons and newly generated hydrocarbons. Previous pyrolysis studies have shown that retained hydrocarbons can contribute substantially to products released during the early heating stage and that their contribution depends on the initial maturity, organic matter type, and experimental system [26]. Therefore, the high oil yields at this stage should not be interpreted solely as newly generated hydrocarbons during laboratory heating.

Between 350 and 475 °C, the oil yields decreased markedly, whereas light hydrocarbons ($C_{6–12}$) and heavy hydrocarbon gases became increasingly important. Propane reached its maximum yield at 425 °C, while ethane and total heavy hydrocarbon gases peaked at 450 °C, and light hydrocarbons reached their maximum yields at 475 °C. These changes reflect a transition from oil-dominated products to increasing contributions from light hydrocarbons and $C_{2–5}$ gases. Previous coal pyrolysis studies have shown that cleavage of aliphatic side chains, decomposition of different organic functional groups, and secondary cracking of retained liquid hydrocarbons may contribute to hydrocarbon generation over this temperature interval [14,24].

At temperatures above 475 °C, methane became progressively dominant among the hydrocarbon products. Methane yields continued to increase, whereas the yields of oil, light hydrocarbons, and heavy hydrocarbon gases generally declined. Meanwhile, the drying coefficients of both samples increased rapidly and approached 100% at 600 °C. The concurrent decrease in liquid hydrocarbons and heavy hydrocarbon gases, together with the continuous increase in methane, is consistent with enhanced secondary cracking and further transformation of residual organic matter at elevated temperatures. Late-stage gas generation may involve overlapping contributions from mature kerogen, retained oil, and further cracking of $C_{2–5}$ gases [27,28].

Although the two coals differed in gas generation intensity, they followed a similar overall hydrocarbon generation sequence, from an interval dominated by oil, through an intermediate interval characterized by light hydrocarbons and heavy hydrocarbon gases, to an interval dominated by methane. The main differences between C-1 and C-2 were reflected in the magnitude and temperature distribution of gas yields, rather than in the overall sequence of product evolution.

4.3. Carbon Isotope Evolution

The carbon isotopic compositions of the hydrocarbon gases generated from C-1 and C-2 showed similar temperature-dependent variations. At the beginning of heating, the recovered gases were likely influenced by both hydrocarbons retained in the coal during previous geological evolution and newly generated pyrolysis gases. Both samples had reached an early maturity stage before the experiments, and C-2 had a relatively high S1 value, suggesting a greater contribution from pre-existing hydrocarbons during the initial heating stage. At approximately 300–350 °C, the release of these retained components may have overlapped with the initial decomposition of coal organic matter. As the temperature increased from 350 to 425 °C, hydrocarbon gas generation intensified, and newly generated gases gradually became dominant. During this interval, decomposition of relatively labile organic structures and cracking of retained liquid hydrocarbons may have contributed to the generation of isotopically lighter gases. Kinetic isotope fractionation during bond cleavage may also favor the release of ^{12}C-enriched products, consistent with the progressive decrease in $\delta^{13}C_1$, $\delta^{13}C_2$, and $\delta^{13}C_3$ values to their minima at approximately 425 °C [24,29].

A clear change occurred after 425 °C. Propane reached its maximum yield at 425 °C, while ethane and total heavy hydrocarbon gases peaked at approximately 450 °C and then declined rapidly. Methane, in contrast, continued to increase. Previous studies have shown that secondary cracking of retained oil and $C_{2–5}$ gases becomes increasingly important at elevated temperatures [24,30], which is consistent with the continued increase in methane and the enrichment of $\delta^{13}C_1$ and $\delta^{13}C_2$ observed here. Preferential release of ^{12}C-enriched products may leave the residual organic matter relatively enriched in ^{13}C, and continued decomposition of this residual material may therefore contribute to isotopically heavier gases [24]. Cleavage of methyl groups from aromatic structures may provide an additional source of methane at higher temperatures [30]. Similar lighter-to-heavier changes in alkane

gas $\delta^{13}C$ values have also been observed in thermal simulation experiments [31], suggesting that the non-monotonic isotope evolution may reflect changes in the relative contributions of different gas-generating components and reactions. In the present experiments, however, both samples maintained the normal carbon isotope sequence of $\delta^{13}C_1 < \delta^{13}C_2 < \delta^{13}C_3$ when complete $C_{1–3}$ isotope data were available, indicating that this non-monotonic evolution is different from carbon isotope series reversal.

Figure 9 places the experimental isotope evolution and fractionation in a broader geological context. Most natural gases from the Huanghua Depression plot within the normal isotope-ordering fields in both the $\delta^{13}C_1$–$\delta^{13}C_2$ and $\delta^{13}C_2$–$\delta^{13}C_3$ diagrams, and their $\delta^{13}C_1$–$\delta^{13}C_2$ distribution is mainly associated with Type III organic matter, consistent with the predominance of Upper Paleozoic coal-bearing source rocks in the depression [17,32]. This distribution is consistent with the normal carbon isotope sequence observed for C-1 and C-2, indicating that the experimental results are broadly comparable with the dominant isotopic characteristics of natural gases in the Huanghua Depression. In contrast, some gases from the Ordos, Sichuan, Fort Worth, and Arkoma basins approach or enter the isotope-reversal fields. Such isotope reversals have been related to continued thermal evolution, secondary cracking, mixing of gases generated at different stages, and post-generation modification [18,31,33,34]. The cross-basin comparison further suggests that non-monotonic changes in individual $\delta^{13}C$ values do not necessarily result in reversal of the $C_{1–3}$ isotope sequence, whereas isotope reversal generally reflects more complex thermal evolution or post-generation processes. Carbon isotope evolution and fractionation can therefore provide useful constraints on gas generation and thermal evolution processes, although their geological interpretation should also consider source type, gas mixing, migration, and reservoir modification.

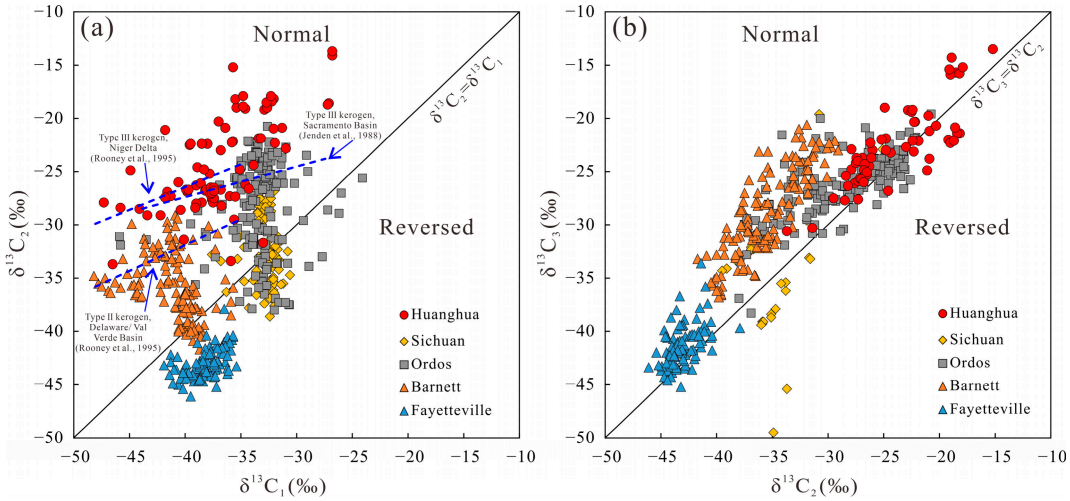

Figure 9. Cross plots of alkane gas carbon isotope compositions from the Huanghua Depression and selected sedimentary basins. (**a**) $\delta^{13}C_1$ versus $\delta^{13}C_2$; (**b**) $\delta^{13}C_2$ versus $\delta^{13}C_3$. Symbols represent different basins as shown in the legend; solid lines mark the isotope ordering boundaries, and dashed lines in (**a**) indicate Type II and Type III kerogen trends. Data sources: [17,24,33,35–38].

4.4. CO2 Generation Potential and Isotopic Constraints

Carbon dioxide in natural gas is controlled by the type of organic matter and thermal maturity. It is a major product of organic matter pyrolysis and one of the most important non-hydrocarbon products in hydrocarbon generation thermal simulation experiments [39]. The relative abundance of CO_2 in this coal pyrolysis experiment decreased sharply between 300 and 450 °C and remained relatively low at higher temperatures (Figure 7). Its yield, however, increased overall with pyrolysis temperature and reached 24.93 mL/g TOC for

C-1 and 32.12 mL/g TOC for C-2 at 600 °C. At relatively low temperatures, CO_2 generation is commonly associated with decarboxylation and decomposition of oxygen-containing functional groups, including carboxyl, carbonyl, and ether structures in coal organic matter. At higher temperatures, further decomposition of residual oxygen-bearing structures may continue to generate CO_2 [14,40]. Its declining proportion in the gaseous products therefore mainly reflects the more rapid increase in methane generation rather than a decrease in its absolute yield. Alongside this shift toward methane-dominated gas, H_2 yields gradually increased at elevated temperatures, which may be related to enhanced dehydrogenation, aromatization, and condensation during continued thermal transformation of the residual coal organic matter [14].

CO_2 generated during pyrolysis may undergo further transformation in the closed high-temperature system, although the specific secondary reaction pathways were not directly evaluated in this study. The $\delta^{13}C_{CO2}$ values of C-1 and C-2 ranged from −19.86‰ to −16.01‰ and from −18.02‰ to −15.48‰, respectively, becoming progressively heavier up to approximately 400 °C and then slightly lighter at higher temperatures. Comparable changes in CO_2 isotope composition have been associated with variations in the relative contributions of different oxygen-bearing organic structures during thermal evolution [40–42]. The measured isotope ranges are broadly consistent with CO_2 derived from the thermal decomposition of organic matter [40,43,44].

The present experiments mainly record the thermogenic generation and transformation of CO_2 in a closed coal pyrolysis system, whereas CO_2 in natural coalbed gas reservoirs is further controlled by microbial activity, groundwater circulation, water–rock reactions, gas migration, and preservation. Hydrogeological conditions in the southern Junggar Basin have been shown to influence both coalbed-gas preservation and microbial CO_2 reduction [45], while studies from the Miquan region indicate that salinity, nutrient availability, groundwater residence time, and hydrodynamic conditions can affect microbial methanogenesis and the preservation of CO_2-rich gas [46]. Regional studies have also shown that coalification-derived CO_2 may be further modified by microbial production and consumption, external carbon input, and differential preservation [47]. Recent syntheses of natural gas reservoirs further demonstrate that CO_2 may originate from organic matter degradation, microbial processes, carbonate decomposition, mantle-derived fluids, and secondary reservoir modification [42]. Thus, the abundance of CO_2 in natural gas reflects not only its original generation from coal organic matter but also its subsequent modification, migration, and preservation in the reservoir.

5. Conclusions

(1) The two coal samples showed similar maximum liquid hydrocarbon yields but different gas yields under the same experimental conditions. The maximum oil yields were 81.94 and 85.08 mg/g TOC for C-1 and C-2, respectively, while the maximum light hydrocarbon yields were 9.64 and 9.97 mg/g TOC. In contrast, C-2 generated more hydrocarbon gas, with a total $C_{1–5}$ yield of 189.69 mL/g TOC, compared with 163.07 mL/g TOC for C-1. The difference between the two samples was more pronounced in gas yields than in liquid hydrocarbon yields.

(2) Both coals followed a similar hydrocarbon generation sequence with increasing pyrolysis temperature. Hydrocarbon generation progressed from an oil-dominated interval at 300–350 °C, through a transitional interval at 350–475 °C characterized by increasing contributions from light hydrocarbons and heavy hydrocarbon gases, to a methane-dominated interval above 475 °C. Despite differences in gas yields, the two samples showed similar overall product evolution sequences.

(3) The alkane gas carbon isotopic compositions showed a similar non-monotonic trend with increasing pyrolysis temperature. The $\delta^{13}C_1$, $\delta^{13}C_2$, and $\delta^{13}C_3$ values became progressively lighter up to approximately 425 °C and then shifted toward heavier values with further heating, while maintaining the normal isotope ordering of $\delta^{13}C_1 < \delta^{13}C_2 < \delta^{13}C_3$. These changes are consistent with variations in the relative contributions of retained hydrocarbons, newly generated gases, secondary cracking products, and residual coal organic matter during pyrolysis.

(4) CO_2 was the dominant non-hydrocarbon gas generated from both coals, whereas H_2 and H_2S remained minor components. Although CO_2 yields increased with increasing temperature, its relative contribution decreased as methane generation increased more rapidly. The relatively narrow $\delta^{13}C_{CO2}$ ranges are broadly consistent with CO_2 derived from the thermal decomposition of organic matter.

Author Contributions: J.X.: Writing—original draft, Visualization, Validation, Methodology, Investigation. Y.L.: Writing—review & editing, Supervision, Resources, Project administration. W.X.: Visualization, Software. J.C.: Resources. W.Z.: Resources. All authors have read and agreed to the published version of the manuscript.

Funding: This study was supported by the Fundamental and Interdisciplinary Disciplines Breakthrough Plan of the Ministry of Education of China (JYB2025XDXM302) and the Fundamental Research Funds for the Central Universities (Ph.D. Top Innovative Talents Fund of CUMTB) (BBJ2025106).

Institutional Review Board Statement: Not applicable.

Informed Consent Statement: Not applicable.

Data Availability Statement: The original contributions presented in this study are included in the article. Further inquiries can be directed to the corresponding author.

Acknowledgments: The authors sincerely thank the anonymous reviewers for their constructive comments and suggestions, which helped improve the quality of this manuscript. The authors also acknowledge the Key Laboratory of Petroleum Geochemistry, Research Institute of Petroleum Exploration and Development, PetroChina, for providing experimental support for the gold-tube pyrolysis and gas geochemical analyses.

Conflicts of Interest: The authors declare no conflicts of interest.

References

1. Li, Y.; Pan, S.; Ning, S.; Shao, L.; Jing, Z.; Wang, Z. Coal Measure Metallogeny: Metallogenic System and Implication for Resource and Environment. *Sci. China Earth Sci.* **2022**, *65*, 1211–1228. [CrossRef]
2. Li, G.; Jia, C.; Zhao, Q.; Zhou, T.; Gao, J. Coal-Rock Gas Accumulation Mechanism and the Whole Petroleum System of Coal Measures. *Pet. Explor. Dev.* **2025**, *52*, 33–49. [CrossRef]
3. Zou, C.; Lin, M.; Ma, F.; Liu, H.; Yang, Z.; Zhang, G.; Yang, Y.; Guan, C.; Liang, Y.; Wang, Y.; et al. Development, Challenges and Strategies of Natural Gas Industry under Carbon Neutral Target in China. *Pet. Explor. Dev.* **2024**, *51*, 476–497. [CrossRef]
4. Zou, C.; Chen, Y.; Kong, L.; Sun, F.; Chen, S.; Dong, Z. Underground Coal Gasification and Its Strategic Significance to the Development of Natural Gas Industry in China. *Pet. Explor. Dev.* **2019**, *46*, 205–215. [CrossRef]
5. He, K.; Zhang, S.; Mi, J.; Zhang, W. Pyrolysis Involving N-Hexadecane, Water and Minerals: Insight into the Mechanisms and Isotope Fractionation for Water-Hydrocarbon Reaction. *J. Anal. Appl. Pyrolysis* **2018**, *130*, 198–208. [CrossRef]
6. Peng, W.; Hu, G.; Liu, Q.; Jia, N.; Fang, C.; Gong, D.; Yu, C.; Lyu, Y.; Wang, P.; Feng, Z. Research Status on Thermal Simulation Experiment and Several Issues of Concern. *J. Nat. Gas Geosci.* **2018**, *3*, 283–293. [CrossRef]
7. Khairy, A.; Uguna, C.N.; Vane, C.H.; El Diasty, W.S.; Peters, K.E.; Snape, C.E.; Farouk, S.; Meredith, W. The Effect of High Pressure on Hydrocarbon Generation from Type-I Kerogen Source Rocks: Implications for Petroleum System Evolution. *Int. J. Coal Geol.* **2025**, *300*, 104708. [CrossRef]
8. Xie, W.-D.; Fu, X.-F.; Wang, H.-X.; Sun, Y.; Vandeginste, V.; Li, X.-P. Thermal Maturity Effect on the Microscopic Pore Structure and Gas Adsorption Capacity of Shale Gas Reservoirs: A Review. *Pet. Sci.* **2025**, *22*, 3967–3990. [CrossRef]

9. Zhang, X.; Guo, W.; Pan, J.F.; Zhu, C.F.; Deng, S.H. In-Situ Pyrolysis of Oil Shale in Pressured Semi-Closed System: Insights into Products Characteristics and Pyrolysis Mechanism. *Energy* **2024**, *286*, 129608. [CrossRef]
10. Gao, L.; Schimmelmann, A.; Tang, Y.; Mastalerz, M. Isotope Rollover in Shale Gas Observed in Laboratory Pyrolysis Experiments: Insight to the Role of Water in Thermogenesis of Mature Gas. *Org. Geochem.* **2014**, *68*, 95–106. [CrossRef]
11. Mi, J.; Zhang, S.; Su, J.; He, K.; Zhang, B.; Tian, H.; Li, X. The Upper Thermal Maturity Limit of Primary Gas Generated from Marine Organic Matters. *Mar. Pet. Geol.* **2018**, *89*, 120–129. [CrossRef]
12. Mi, J.; Zhang, S.; He, K. Experimental Investigations about the Effect of Pressure on Gas Generation from Coal. *Org. Geochem.* **2014**, *74*, 116–122. [CrossRef]
13. Zhang, S.; Mi, J.; He, K. Synthesis of Hydrocarbon Gases from Four Different Carbon Sources and Hydrogen Gas Using a Gold-Tube System by Fischer–Tropsch Method. *Chem. Geol.* **2013**, *349–350*, 27–35. [CrossRef]
14. He, K.; Zhang, S.; Mi, J.; Zhang, W. The Evolution of Chemical Groups and Isotopic Fractionation at Different Maturation Stages during Lignite Pyrolysis. *Fuel* **2018**, *211*, 492–506. [CrossRef]
15. Liu, Q.Y.; Worden, R.H.; Jin, Z.J.; Liu, W.H.; Li, J.; Gao, B.; Zhang, D.W.; Hu, A.P.; Yang, C. TSR versus Non-TSR Processes and Their Impact on Gas Geochemistry and Carbon Stable Isotopes in Carboniferous, Permian and Lower Triassic Marine Carbonate Gas Reservoirs in the Eastern Sichuan Basin, China. *Geochim. Cosmochim. Acta* **2013**, *100*, 96–115. [CrossRef]
16. Tilley, B.; McLellan, S.; Hiebert, S.; Quartero, B.; Veilleux, B.; Muehlenbachs, K. Gas Isotope Reversals in Fractured Gas Reservoirs of the Western Canadian Foothills: Mature Shale Gases in Disguise. *AAPG Bull.* **2011**, *95*, 1399–1422. [CrossRef]
17. Zhao, X.; Pu, X.; Jiang, W.; Zhou, L.; Jin, F.; Xiao, D.; Fu, L.; Li, H. An Exploration Breakthrough in Paleozoic Petroleum System of Huanghua Depression in Dagang Oilfield and Its Significance, North China. *Pet. Explor. Dev.* **2019**, *46*, 651–663. [CrossRef]
18. Liu, C.; Lei, M.; Sun, B.; Wang, X. Origin and Process of Carbon Isotopic Reversal of Tight Sandstone Gas in the Shixi Gas Field, Eastern Margin of Ordos Basin. *Int. J. Coal Geol.* **2023**, *276*, 104327. [CrossRef]
19. Chang, J.; Qiu, N.; Zhao, X.; Shen, F.; Liu, N.; Xu, W. Mesozoic and Cenozoic Tectono-Thermal Reconstruction of the Western Bohai Bay Basin (East China) with Implications for Hydrocarbon Generation and Migration. *J. Asian Earth Sci.* **2018**, *160*, 380–395. [CrossRef]
20. Yang, R.; Liu, H.; Li, H.; Zhao, C.; Li, C. Accumulation Mechanism and Model of Coal Measure Derived Oil and Gas in the Deep Reservoir of Huanghua Depression, Bohai Bay Basin, China. *J. Nat. Gas Geosci.* **2022**, *7*, 277–293. [CrossRef]
21. Yang, R.; Zhao, X.; Li, H.; Zhao, C.; Pu, X.; Liu, H.; Fu, L.; Li, C. Evolution Characteristics of the Upper Paleozoic Source Kitchen and Its Controlling Effects on Hydrocarbon Accumulation in the Paleozoic Petroleum System in Huanghua Depression, Bohai Bay Basin, China. *J. Pet. Sci. Eng.* **2020**, *193*, 107415. [CrossRef]
22. Ju, Y.; Yu, K.; Wang, G.; Li, W.; Zhang, K.; Li, S.; Guo, L.; Sun, Y.; Feng, H.; Qiao, P.; et al. Coupling Response of the Meso–Cenozoic Differential Evolution of the North China Craton to Lithospheric Structural Transformation. *Earth Sci. Rev.* **2021**, *223*, 103859. [CrossRef]
23. *GB/T 19145-2022*; Determination for Total Organic Carbon in Sedimentary Rock. Standardization Administration of China: Beijing, China, 2022.
24. Ni, Y.; Gao, J.; Chen, J.; Liao, F.; Liu, J.; Zhang, D. Gas Generation and Its Isotope Composition during Coal Pyrolysis: Potential Mechanism of Isotope Rollover. *Fuel* **2018**, *231*, 387–395. [CrossRef]
25. Xu, J.-J.; Jin, Q. Hydrocarbon Generation from Carboniferous-Permian Coaly Source Rocks in the Huanghua Depression under Different Geological Processes. *Pet. Sci.* **2020**, *17*, 1540–1555. [CrossRef]
26. Xiao, J.; Feng, Z.; Qiu, Z.; Zhang, Q.; Li, Y.; Wang, W.; Yang, M. Formation Mechanism of Liquid Hydrocarbon Products of Type III Kerogen: Insights from Temperature-Based Semi-Open Pyrolysis. *Fuel* **2025**, *391*, 134642. [CrossRef]
27. Liu, X.; Wang, Q.; Jia, W.; Song, J.; Peng, P. Pyrolysis of an Organic-Rich Shale Containing Type II Kerogen before and after Oil Generation and Expulsion: Implications for the Generation of Late Hydrocarbon and Hydrogen Gases. *J. Anal. Appl. Pyrolysis* **2023**, *173*, 106105. [CrossRef]
28. Wang, H.; Niu, D.; Luan, Z.; Dang, H.; Pan, X.; Sun, P. Kinetic Characteristics of Secondary Hydrocarbon Generation from Oil Shale and Coal at Different Maturation Stages: Insights from Open-System Pyrolysis. *Int. J. Coal Geol.* **2025**, *308*, 104845. [CrossRef]
29. Peng, W.; Liu, Q.; Hu, G.; Lyu, Y.; Zhu, D.; Meng, Q.; Guo, F.; Wang, R. Mechanisms of Carbon Isotopic Fractionation in the Process of Natural Gas Generation: Geochemical Evidence from Thermal Simulation Experiment. *Pet. Explor. Dev.* **2020**, *47*, 1042–1054. [CrossRef]
30. Zhang, Z.; Zhang, C.; Chen, Y.; Volkman, J.K.; Sun, Y. Generation of Abnormal Distributions of Inter- and Intramolecular δ13C Compositions in Hydrocarbons from Gold Tube Pyrolysis of an Australian Torbanite. *Org. Geochem.* **2024**, *194*, 104813. [CrossRef]
31. Pei, L.; Liu, W.; Guo, Q.; Wang, X.; Luo, H.; Wang, Q. Genetic Significance of Carbon Isotope Curve Types of Methane, Ethane, and Propane in Natural Gas. *Org. Geochem.* **2023**, *186*, 104691. [CrossRef]
32. Rooney, M.A.; Claypool, G.E.; Chung, H.M. Modeling Thermogenic Gas Generation Using Carbon Isotope Ratios of Natural Gas Hydrocarbons. *Chem. Geol.* **1995**, *126*, 219–232. [CrossRef]

33. Zumberge, J.; Ferworn, K.; Brown, S. Isotopic Reversal ('Rollover') in Shale Gases Produced from the Mississippian Barnett and Fayetteville Formations. *Mar. Pet. Geol.* **2012**, *31*, 43–52. [CrossRef]
34. Feng, Z.; Hao, F.; Tian, J.; Zhou, S.; Dong, D.; Huang, S. Shale Gas Geochemistry in the Sichuan Basin, China. *Earth Sci. Rev.* **2022**, *232*, 104141. [CrossRef]
35. Dai, J.; Zou, C.; Dong, D.; Ni, Y.; Wu, W.; Gong, D.; Wang, Y.; Huang, S.; Huang, J.; Fang, C.; et al. Geochemical Characteristics of Marine and Terrestrial Shale Gas in China. *Mar. Pet. Geol.* **2016**, *76*, 444–463. [CrossRef]
36. Dai, J.; Li, J.; Luo, X.; Zhang, W.; Hu, G.; Ma, C.; Guo, J.; Ge, S. Stable Carbon Isotope Compositions and Source Rock Geochemistry of the Giant Gas Accumulations in the Ordos Basin, China. *Org. Geochem.* **2005**, *36*, 1617–1635. [CrossRef]
37. Liu, D.; Zhang, W.; Kong, Q.; Feng, Z.; Fang, C.; Peng, W. Lower Paleozoic Source Rocks and Natural Gas Origins in Ordos Basin, NW China. *Pet. Explor. Dev.* **2016**, *43*, 591–601. [CrossRef]
38. Zhang, S.; He, K.; Hu, G.; Mi, J.; Ma, Q.; Liu, K.; Tang, Y. Unique Chemical and Isotopic Characteristics and Origins of Natural Gases in the Paleozoic Marine Formations in the Sichuan Basin, SW China: Isotope Fractionation of Deep and High Mature Carbonate Reservoir Gases. *Mar. Pet. Geol.* **2018**, *89*, 68–82. [CrossRef]
39. Seewald, J.S.; Benitez-Nelson, B.C.; Whelan, J.K. Laboratory and Theoretical Constraints on the Generation and Composition of Natural Gas. *Geochim. Cosmochim. Acta* **1998**, *62*, 1599–1617. [CrossRef]
40. Shuai, Y.; Zhang, S.; Peng, P.; Zou, Y.; Yuan, X.; Liu, J. Occurrence of Heavy Carbon Dioxide of Organic Origin: Evidence from Confined Dry Pyrolysis of Coal. *Chem. Geol.* **2013**, *358*, 54–60. [CrossRef]
41. Tao, W.; Zou, Y.-R.; Carr, A.; Liu, J.; Peng, P. Study of the Influence of Pressure on Enhanced Gaseous Hydrocarbon Yield under High Pressure–High Temperature Coal Pyrolysis. *Fuel* **2010**, *89*, 3590–3597. [CrossRef]
42. Jiang, M.; Liu, Q.; Wu, X.; Zhu, D. Advancements in Geochemistry and Origins of CO_2 in Natural Gas Reservoirs of China. *Mar. Pet. Geol.* **2025**, *173*, 107267. [CrossRef]
43. Carothers, W.W.; Kharaka, Y.K. Stable Carbon Isotopes of HCO3− in Oil-Field Waters—Implications for the Origin of CO_2. *Geochim. Cosmochim. Acta* **1980**, *44*, 323–332. [CrossRef]
44. Honty, M.; Ostertag-Henning, C.; Koděra, P.; Frederickx, L.; Jacops, E.; Wang, L.; Salah, S.; Sillen, X. The Fate of Carbon Dioxide Generated by Decomposition of the Organic Matter in the Boom Clay upon Heating at 80 °C: The Buffering Role of Carbonates and Implications for the Geological Disposal of Heat-Emitting Waste. *Appl. Geochem.* **2024**, *162*, 105899. [CrossRef]
45. Fu, H.; Tang, D.; Pan, Z.; Yan, D.; Yang, S.; Zhuang, X.; Li, G.; Chen, X.; Wang, G. A Study of Hydrogeology and Its Effect on Coalbed Methane Enrichment in the Southern Junggar Basin, China. *AAPG Bull.* **2019**, *103*, 189–213. [CrossRef]
46. Fu, H.; Li, Y.; Su, X.; Yan, D.; Yang, S.; Wang, G.; Wang, X.; Zhao, W. Environmental Conditions and Mechanisms Restricting Microbial Methanogenesis in the Miquan Region of the Southern Junggar Basin, NW China. *GSA Bull.* **2023**, *135*, 420–434. [CrossRef]
47. Tang, S.; Tang, D.; Tao, S.; Sun, B.; Zhang, A.; Zhang, T.; Pu, Y.; Zhi, Y. CO_2-Enriched CBM Accumulation Mechanism for Low-Rank Coal in the Southern Junggar Basin, China. *Int. J. Coal Geol.* **2022**, *253*, 103955. [CrossRef]